Journal of Catalysis 274 (2010) 11–20

Contents lists available at ScienceDirect

Journal of Catalysis

journal homepage: www.elsevier.com/locate/jcat

Characterization of alumina-supported Pt, Ni and PtNi alloy catalysts for the dry reforming of methane

Mónica García-Diéguez [a], Elisabetta Finocchio [b], María Ángeles Larrubia [a], Luis J. Alemany [a], Guido Busca [b,*]

[a] Departamento de Ingeniería Química, Facultad de Ciencias, Campus de Teatinos, Universidad de Málaga, E-29071 Málaga, Spain
[b] Dipartimento di Ingegneria Chimica e di Processo, Università di Genova, P.le J.F. Kennedy 1, I-16129 Genova, Italy

ARTICLE INFO

Article history:
Received 24 February 2010
Revised 29 April 2010
Accepted 31 May 2010

Keywords:
PtNi alloy catalysts
Alloy catalysts
Ni catalysts
Supported Pt catalysts
Reforming catalysts
Nanostructured alumina
CO adsorption
Dry reforming
IR spectroscopy

ABSTRACT

Two bimetallic PtNi catalysts supported on a nanostructured γ-Al_2O_3 together with the corresponding monometallic materials, employed for the dry reforming of methane, have been prepared and characterized. Characterization of the catalysts, in reduced form, has been performed by FTIR spectroscopy of adsorbed carbon monoxide at low and room temperature. XRD, TEM and XPS analysis have also been performed. IR spectra of adsorbed CO indicate that the surface of the PtNi catalysts is dominated by Pt centers, whose electron-withdrawing character is increased by Ni. It has also been confirmed the formation of PtNi alloy, which is enriched at the surface by Pt and has smaller metal crystal size than metal particles in monometallic Pt and Ni catalysts. The alloy formation is associated with higher activity and lower production of carbonaceous materials upon dry reforming of methane.

1. Introduction

Hydrogen is mostly produced today through steam reforming of hydrocarbons, usually natural gas [1,2], performed at 1000–1200 K. The industrial catalysts are invariably based on Ni supported on an alumina-based carrier, usually stabilized by the presence of alkali and/or alkali earth cations [1–4]. These catalysts can be prepared by different methods such as impregnation of pre-synthesized supports or by different coprecipitation procedures [3,4]. Slow coking of these catalysts gives rise to deactivation, although regeneration is possible. These catalysts, however, are reported to be rapidly irreversibly deactivated in case of daily start-up and shut-down operation, typical in case of hydrogen and fuel cells domestic use. In this case, Ni catalysts doped with small amounts of noble metals are reported to display an "intelligent" behavior, with suppression of such deactivation phenomena [5].

Similar Ni-based catalysts are also proposed for the development of processes for the production of hydrogen from renewables [6] such as bioethanol [7–11], acetic acid [12–14] and glycerol [15], which would result in the release of the energy production from fossil fuels and, simultaneously, in the reduction of greenhouse gases emissions. However, at least in the case of ethanol steam reforming, cobalt–nickel bimetallic catalysts appear to be more efficient than Ni catalysts [16,17].

The production of low H_2/CO ratio syngases through the dry reforming of methane, i.e. the reaction of methane with carbon dioxide, is also a potentially useful process. Coking in this case is a more serious problem, and for this reason, noble metal catalysts, which suffer coking less than Ni-based ones, have longer life [18–20]. Also in this case, bimetallic catalysts, such as Pt-doped Ni catalysts, may have optimal behavior [21].

Pt/Al_2O_3 catalysts are also quite largely used as dehydrogenation catalysts such as in the Oleflex light paraffin dehydrogenation technology and in the Pacol long linear paraffin dehydrogenation technology, both from UOP [22]. Similar catalysts are used in the hydrogenation reactions, e.g. for isooctene hydrogenation to isooctane and dearomatization reactions [23], as well as in the BenSat benzene saturation technology from UOP [24]. In contrast, Ni/Al_2O_3 catalysts find large industrial application as hydrogenation catalysts such as for methanation and substitute natural gas synthesis [25,26], as well as for the dearomatization and desulfurization of hydrocarbon feeds. In general, one of the reasons of choice between Pt- and Ni-based catalysts is the resistance to sulfur compounds, rather than their catalytic activity.

In this work, two bimetallic combinations of PtNi have been prepared, supported over nanostructured γ-Al_2O_3 together with

* Corresponding author.
E-mail address: Guido.Busca@unige.it (G. Busca).

0021-9517/$ - see front matter © 2010 Elsevier Inc. All rights reserved.
doi:10.1016/j.jcat.2010.05.020

the corresponding monometallic materials. These catalysts have been characterized for their metal particle size and metal textural properties (with respect to the pure support and the corresponding monometallic materials). This work is part of an investigation aimed at the development of efficient catalysts for syngas production by methane dry reforming.

2. Experimental

2.1. Catalysts preparation

A synthesized nanostructured γ-Al_2O_3 was employed as support. The nanostructured alumina was prepared using $NaAlO_2$ as precursor. An aqueous $NaAlO_2$ solution was added dropwise to 5 N acetic acid solution. The precipitate obtained was decanted, filtered and washed with water. The resulting powder was dried overnight at 100 °C and subsequently mixed with a non-ionic surfactant (Tergitol 15-TS-5, Sigma) using a Tergitol/Al ratio of 0.5. The mixture was maintained in an autoclave for 72 h at 100 °C and later calcined at 500 °C for 20 h. Before the catalysts preparation, the support was calcined in air at 800 °C for 2 h (10 °C/min).

Bimetallic supported catalysts (Pt [0.04, 0.4 at/nm^2]–Ni [4 at/nm^2], corresponding to 0.4 or 4 wt% Pt, 10 wt% Ni) denoted as xPt4Ni/Al_2O_3, where x is the Pt load (expressed in terms of calculated virtual atomic superficial density), were prepared by simultaneous incipient wetness impregnation of the support, with a solution of diaminedinitroplatinum and/or nickel nitrate. The impregnation was done in a single step. The support impregnated was dried at 100 °C for 2 h and calcined at 600 °C for 2 h (10 °C/min). Monometallic catalysts (Pt [0.4 at/nm^2], corresponding to 4 wt% Pt, and Ni [4 at/nm^2], corresponding to 10 wt% Ni; denoted as 0.4Pt/Al_2O_3 and 4Ni/Al_2O_3, respectively) were also prepared. In Table 1, data on the catalysts investigated here are summarized.

2.2. Catalytic measurements

Reactivity experiments were carried out in a Microactivity-Reference reaction system from PID Eng&Tech (Spain) at atmospheric pressure (650–700 °C). A tubular fixed-bed stainless steel reactor (i.d. 9 mm) with 100 mg of catalyst (250–420 μm) was employed. The total gas flow rate was kept constant at 50 Ncm^3/min with composition: CH_4/CO_2/He = 20/20/60. The space velocity and the contact time were 6000 h^{-1} and 0.8 g h mol^{-1}, respectively, operating under plug flow conditions. Preliminary reactivity tests with different catalyst particle sizes and dilutions, measuring the radial and axial temperatures at different points, were performed to confirm the non-existence of heat or mass transfer limitations. Before reaction, catalysts were activated *in situ* with H_2 (3% in He, 30 Ncm^3 min^{-1}) at 700 °C for 2 h. The reaction temperature was measured with a thermocouple placed in the reactor bed. The reactor effluent was analyzed by GC (Agilent 4890D) equipped with TCD and FID detectors. Stability runs were performed at 700 °C, where the highest formation of carbon is expected.

2.3. Catalysts characterization

FTIR spectra of self-supporting catalyst disks have been recorded by a Thermofisher 380 Instrument. Pure powders have been reduced in hydrogen at 773 K and outgassed at the same temperature before each adsorption experiment. CO adsorption has been performed both at room temperature and liquid nitrogen temperature. These experiments could not be done with Ni-containing spent catalysts because of the carbonaceous material that hinders the preparation of thin pressed disks and causes full absorption of the IR light.

X-ray powder diffraction data have been recorded with an X'Pert MPD PRO diffractometer (PANalytical) using Cu Kα1 radiation (λ = 1.54059 Å) and a Ge (1 1 1) primary monochromator. The X-ray tube worked at 45 kV and 35 mA. The measurements were done from 20° to 70° (2θ).

The carbon content of the catalysts after reaction was obtained *via* elemental analysis technique using an Elemental Analyzer Perkin-Elmer 2400 CHN.

Photoelectron spectra were recorded over fresh samples using a Physical Electronic 5700 spectrometer equipped with a hemispherical electron analyzer operating with a Mg Kα X-ray exciting source (1253.6 eV, 15 kV, 300 W). The binding energies (BE) were referenced to the C_{1s} peak, used as an internal patron for calibration and fixed at 284.8 eV considering a deviation ±0.2 eV. All deconvolutions of experimental curves were done with Gaussian and Lorenzian line fitting, minimizing the (χ^2) chi-square values. The references values were taken from the NIST X-ray photoelectron spectroscopy database [27].

TEM images were taken with a Philips CM 200 of 200 kV, coupled with EDX microanalysis; the samples were prepared using ethanol as dispersant.

3. Results

3.1. Catalytic activity measurements

The activity of the catalysts has been described in detail in [28]. The CO_2 and CH_4 conversion values obtained with the catalyst at 650 °C and at 700 °C are presented in Table 2. The CO_2 conversion values are higher than those of methane, due to the presence of side reactions, such as the reverse water gas shift reaction and the Boudouard reaction. In agreement with this, the H_2/CO ratio values reached with all of the catalysts are similar, between 0.64 and 0.68 (Table 2). The activity of the 0.04Pt4Ni/Al_2O_3 catalyst does not present significant modifications with respect to the monometallic Ni catalyst. The conversion of both methane and CO_2 is maximum for the 0.4Pt4Ni/Al_2O_3 catalyst.

In Table 2, the CO_2 conversion loss expressed as conversion loss per hour of time-on-stream (% h^{-1}) over the catalysts under study working at 700 °C are also shown, as a rough measure of deactivation kinetics. It is evident that the deactivation rate decreases strongly by the addition of Pt to Ni/Al_2O_3 catalyst. Indeed, the

Table 1
Theoretical metal content and atomic metal density of the catalysts.

Catalyst	Metal density (at/nm^2)		Metal content (wt%)		Pt/Ni[a]	Superficial metal content[b] (wt%)	
	Ni	Pt	Ni	Pt		Ni	Pt
4Ni/Al_2O_3	4	0	10	0	0	8	0
0.04Pt4Ni/Al_2O_3	4	0.04	10	0.4	1/100	8	1
0.4Pt4Ni/Al_2O_3	4	0.4	10	4	1/10	9	3
0.4Pt/Al_2O_3	0	0.4	0	4	∞	0	2

[a] Theoretical atomic ratio.
[b] Measured atomic superficial concentration (XPS).

Table 2
Catalytic activity data.

Catalyst	XCO_2[a] (%)		XCH_4[b] (%)		H_2/CO		XCO_2 loss[c]
	650 °C	700 °C	650 °C	700 °C	650 °C	700 °C	(% h^{-1})
$4Ni/Al_2O_3$	50	70	39	60	0.66	0.66	1.4
$0.04Pt4Ni/Al_2O_3$	52	70	41	60	0.65	0.64	0.4
$0.4Pt4Ni/Al_2O_3$	59	76	48	69	0.65	0.66	0.3
$0.4Pt/Al_2O_3$	54	76	42	65	0.64	0.68	0.3

$CO_2/CH_4/He$ = 1/1/3, GHSV = 6000 h^{-1}, W/F = 0.8 g h mol^{-1} and atmospheric pressure, up to 14-h time-on-stream.
[a,b] CO_2 and CH_4 conversion values.
[c] CO_2 conversion loss (700 °C).

Pt-containing catalysts supported on the fibrous alumina are rather stable for the DRM. This is in agreement with literature data showing that on Pt/Al_2O_3 catalysts, carbon is removed by oxidation by CO_2 [29], ensuring a longer accessibility to active Pt sites.

3.2. XRD patterns

In Fig. 1, the XRD patterns of the samples under study, after reaction in methane dry reforming, are reported. Here, a slightly different interpretation of the XRD pattern is reported with respect to the previous one [28]. In both cases of pure supported metal catalysts, the XRD diffraction peaks of the corresponding face-centered cubic phase (cF4, space group $Fm^{-}3m$) are observed, as expected indeed. In particular, we observe the [1 1 1] and the [2 0 0] peaks for both pure phases, whose position is reported in Table 3. Also, in the case of sample $0.04Pt4Ni/Al_2O_3$, the peaks of metallic Ni are evident, apparently not shifted, but lowered in intensity and broadened very much. This is an indication of the formation of smaller crystals, as deduced by the crystal size calculation made using the Scherrer equation. In the case of the $0.4Pt4Ni/Al_2O_3$ sample, the [1 1 1] and [2 0 0] peaks of nickel metal are very much broadened but also definitely displaced to lower 2θ values. This corresponds to a further important lowering of the crystal size but also to a modification of the unit cell dimensions. From the position of the [2 0 0], peak is possible to calculate that the increase in the Ni fcc unit cell dimension in the case of the $0.4Pt4Ni/Al_2O_3$ sample is roughly 10% the difference between the cell dimensions of the Pt and Ni monometallic catalysts, which is in rough agreement with the Vegard's law for substitutional solid solutions, taking into account that the Pt molar fraction of this sample is 0.09 (assuming both Pt and Ni fully reduced and excluding alumina). These data show that in the case of the $0.4Pt4Ni/Al_2O_3$ sample, a fcc substitutional solid solution is formed. In fact, it is well known that a partial solubility exists at temperatures below 900 K in the fcc phase between Ni and Pt. The solubility of Pt in Ni fcc decreases by decreasing temperature being near 15% mol at 650 K [30]. At higher Pt contents, three different intermetallic phases become thermodynamically stable, Ni_3Pt, NiPt and $NiPt_3$. The composition of the $0.4Pt4Ni/Al_2O_3$ sample is near the limit of thermodynamic stability of the disordered fcc solid solution at r.t. On the other hand, in our experimental conditions, the disordered fcc solid solution can be distinguished with difficulty from the ordered Ni_3Pt intermetallic phase (Cu_3Au-type, $L1_2$ structure; space group Pm 3m). In fact, the weak superlattice [1 1 0], [2 1 0] and [2 1 1] peaks (not found in our XRD pattern) are expected weak and further weakened and broadened due to the very small crystal size of such a metallic phase. The [1 1 1] and [2 0 0] interplanar distances we measure here for the $0.4Pt4Ni/Al_2O_3$ sample (Table 3)

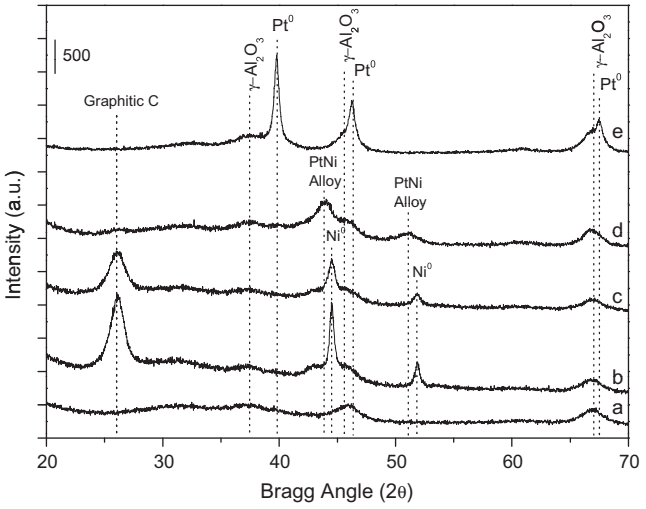

Fig. 1. XRD patterns of fibrous alumina support (a), spent $4Ni/Al_2O_3$ (b), spent $0.04Pt4Ni/Al_2O_3$ (c), spent $0.4Pt4Ni/Al_2O_3$ (d), and spent $0.4Pt/Al_2O_3$ (e).

Table 3
Analysis of metal particles in spent catalysts by XRD.

Catalyst	XRD data				TEM data		EA data
	2θ	d[a] (Å)	$D_P Ni^{0}$[b] (nm)	$D_P Pt^{0}$[b] (nm)	$D_P Ni^{0}$ (nm)	$D_P Pt^{0}$ (nm)	C[c] (wt%)
$0.4Pt/Al_2O_3$	39.8 [1 1 1]	2.26				10–20	1
	46.3 [2 0 0]	1.96		11			
$0.4Pt4Ni/Al_2O_3$	43.9 [1 1 1]	2.06	–		10		6
	51.2 [2 0 0]	1.78	7				
$0.04Pt4Ni/Al_2O_3$	44.5 [1 1 1]	2.03	–		14		36
	51.8 [2 0 0]	1.76	13				
$4Ni/Al_2O_3$	44.5 [1 1 1]	2.03	–		25		45
	51.8 [2 0 0]	1.76	23				

[a] Spacing between the planes.
[b] Average particle size, calculated by the Scherrer equation.
[c] Carbon content in spent catalysis, obtained by elemental analysis.

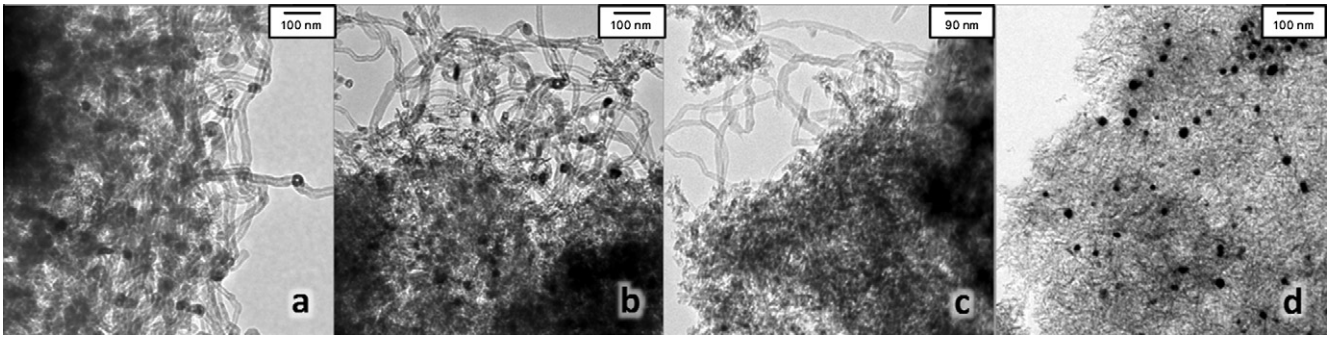

Fig. 2. TEM micrographs of (a) spent $4Ni/Al_2O_3$, (b) spent $0.04Pt4Ni/Al_2O_3$, (c) spent $0.4Pt4Ni/Al_2O_3$, and (d) spent $0.4Pt/Al_2O_3$.

Table 4
BE and surface atomic ratios of catalysts before reaction (BR) and after reaction (AR).

Catalyst	Ni $2p_{3/2}$*			Pt $4d_{5/2}$*		
		BR	AR		BR	AR
$4Ni/Al_2O_3$	Ni^0	–	852.9 (25)	–	–	–
	NiO	855.3 (32)	854.6 (25)	–	–	–
	$NiAl_2O_4$	856.1 (68)	856.1 (50)	–	–	–
	*Ni/Al***	0.09	0.02	–	–	–
$0.04Pt4Ni/Al_2O_3$	Ni^0	–	853.1 (32)	Pt^0	314.2 (21)	314.6 (100)
	NiO	855.2 (34)	854.7 (20)	PtO	317.8 (79)	
	$NiAl_2O_4$	856.4 (66)	856.2 (48)			
	*Ni/Al***	0.09	0.03	*Pt/Al***	0.002	0.002
$0.4Pt4Ni/Al_2O_3$	Ni^0	–	853.1 (35)	Pt^0	314.9 (42)	314.6 (100)
	NiO	855.2 (39)	855.0 (20)	PtO	317.5 (58)	–
	$NiAl_2O_4$	856.5 (61)	856.6 (45)			
	*Ni/Al***	0.1	0.06	*Pt/Al***	0.01	0.01
$0.4Pt/Al_2O_3$	–	–	–	Pt^0	314.9 (87)	314.2 (100)
	–	–	–	PtO	317.4 (13)	–
	–	–	–	*Pt/Al***	0.01	0.01

* Binding energies (±0.2 eV), in brackets () relative population of the species expressed in %.
** Surface atomic ratio.

are smaller than those measured for Ni_3Pt particles supported on silica [31], suggesting that the Ni–Pt ratio in this phase may be, in our case, larger than 3. The formation of Ni–Pt alloys has already been determined by different techniques for silica-supported catalysts, where, depending on the composition, ordered PtNi intermetallic and disordered fcc solid solution were found to exist or coexist [32–34].

In the case of spent Ni-containing catalysts, an additional XRD peak is observed, which can be confidently assigned to graphitic carbon. In fact, it is well known that Ni-based catalysts tend to form carbonaceous materials under steam-reforming conditions, producing "carbon whiskers" or nanotubes [1–5], as well as, possibly, other forms of carbonaceous materials. It is evident from the XRD pattern that the amount of graphitic carbon strongly decreases by adding Pt to Ni on the catalyst, in agreement with the carbon content in the catalysts after reaction obtained by elemental analysis (see Table 3).

3.3. TEM Micrographs and XPS study

The TEM micrographs of the samples registered after reaction are compared, at the same magnification, in Fig. 2. The TEM micrograph of the $0.4Pt/Al_2O_3$ catalyst clearly shows the typical fibrous particles of the alumina support together with evident metallic particles. In the case of the three Ni-containing catalysts, carbon nanotubes are also very evident, as a typical behavior of Ni catalysts under reforming conditions. The amount of carbon whiskers definitely decreases by increasing the Pt content of Ni-containing catalysts, and possibly also the nature and thickness of their walls seems to be modified. However, Ni metal particles are also evident, in particular for the $4Ni/Al_2O_3$ and the $0.04Pt4Ni/Al_2O_3$ catalysts. In Table 3, the size of the metallic crystals as observed by XRD and TEM are compared.

In Table 4, the XPS peaks observed for the catalysts discharged under nitrogen (with a minimum contact with air) after reaction are summarized and compared with the data for the fresh catalysts. The data indicate that the $4Ni/Al_2O_3$ catalyst is only partially reduced after reaction, the most abundant species at the surface being Ni aluminate, together with NiO. On the contrary, the monometallic $0.4Pt/Al_2O_3$ catalyst is fully reduced, as expected indeed due to its noble metal character. In the case of bimetallic catalysts, the reduction of Ni increases slightly, while Pt is still fully reduced after reaction. It is interesting to remark that, based on XPS data, the composition of the $0.4Pt4Ni/Al_2O_3$ catalyst in terms of metallic elements at the reduced state is out of the stability range of disordered fcc solid solution, entering in the stability range of the ordered Ni_3Pt intermetallic compound. In fact, the molar ratio between Ni and Pt metals is, based on these data, a little higher than 3. As said, in our conditions it is certainly difficult to detect superlattice XRD peaks. Actually, a kinetic, rather a thermodynamic, control of the metallic phase crystallization in the preparation and reaction conditions of our catalysts may occur. In any case, the XPS data indicate that all Ni-containing catalysts are only partially reduced even after reaction.

3.4. IR study of CO adsorption over the 0.4Pt/Al_2O_3 catalyst

The characterization after reaction shows that in particular 4Ni/Al_2O_3 and 0.04Pt4Ni/Al_2O_3 catalysts are partially reduced and covered by carbon nanotubes. To allow IR study, we decided to make this characterization on samples that underwent mild reduction by hydrogen in the IR cell, to avoid formation of carbonaceous materials.

The spectra of CO absorbed over the reduced 0.4Pt/Al_2O_3 catalyst, at low temperature are shown in Fig. 3, left. At the highest CO coverage (−140 °C), a main band is observed at 2069 cm^{-1} with a broad weaker band centered at 1794 cm^{-1}. The positions and relative intensities of these bands are typical for CO adsorption on Pt metal particles, where terminal carbonyls (absorbing at 2050–2100 cm^{-1}) usually largely predominate over bridging ones (absorbing at lower frequencies, see Ref. [35] and references therein).

Two additional sharp weak bands are observed in the presence of the gas, at 2186 and 2161 cm^{-1}, but disappear upon outgassing. These bands fall in the typical region of CO stretchings of CO interacting with metal cations [36]. The band at 2186 cm^{-1} is assigned to CO σ-bonded to Al^{3+} ions exposed on the support surface, while the one at 2161 cm^{-1} might be due to species interacting with surface hydroxy groups. However, an assignment of the last species to CO interacting with oxidized Pt centers, likely Pt^{2+}–CO species, cannot be completely ruled out.

Outgassing upon warming causes a slight shift of the main maximum from 2069 to 2055 cm^{-1}, and also a very slight shift of the band at 1794 cm^{-1} to lower frequencies. However, both bands do not decrease significantly in intensity.

The spectra of surface species arising from CO adsorption over the reduced 0.4Pt/Al_2O_3 catalyst, at room temperature, are presented in Fig. 3, right. In contact with the gas, the largely predominant band is centered at 2064 cm^{-1}, still in the region of terminal carbonyls, while the band of bridging species is observed at 1815 cm^{-1}. The latter disappears faster than the former during outgassing upon heating, in agreement with the lower stability of bridging carbonyls on most Pt single crystal faces (such as Pt{1 1 1} and Pt{1 1 0}), as well as on its steps [37].

Although the assignment of these two adsorptions to terminal and bridging species is straightforward, their position and their shape deserve some discussion. Indeed, the position of the lower frequency band is definitely at lower frequency than for typical bands of bridging carbonyls on Pt crystals, usually in the range 1910–1840 cm^{-1} on both low-index faces and stepped faces, suggesting a possible assignment to triply bridging species.

On the other hand, also the band of terminal carbonyls is quite broad, clearly showing a sharp component at higher frequencies (2075 cm^{-1}) and a broad one at lower frequencies (1970 cm^{-1}). After outgassing at room temperature, the maximum slightly shifts to 2058 cm^{-1}, the highest frequency component becoming more evident, but the band does not change its relative intensity. After outgassing upon warming (Fig. 3, right (c–g)), the band of linear carbonyls decreased in intensity and disappeared at 400 °C. Additionally, the maximum significantly shifted downwards to 2032 cm^{-1}, the two shoulders still appearing more pronounced at the low (1970 cm^{-1}) and high (2058 cm^{-1}) frequency sides. We can propose that we have again two families of terminal carbonyl species (2058, 2032 cm^{-1}) and the anomalous formation of bridging species (1971 cm^{-1}) during outgassing upon heating.

This picture shows the presence of different kinds of Pt-adsorbing carbon monoxide.

The adsorption modes of CO on low-index platinum monocrystal surfaces have been reviewed some years ago by Curulla et al. [35]. At low coverages, both on Pt{1 1 1} and on Pt{1 1 0} monocrystal faces, only one band is observed by IRAS and/or EELS techniques due to CO adsorbed on atop sites. According to Crossley and King [38], this band shifts from 2063 cm^{-1} at the lowest coverages to 2100 cm^{-1} at saturation on Pt{1 1 1}. Using sum-frequency generation spectroscopy (SFG), this band was found to shift from 2090 to 2105 cm^{-1} when CO pressure increases from 10^{-7} to 500 mbar at 300 K on Pt{1 1 1} [39]. Klünker et al. [40] observed this band shifting from 2065 to 2088 cm^{-1} on Pt{1 1 0}.

These bands have been assigned to isolated CO molecules on reconstructed Pt{1 1 0}-(1×2) face and on the $\sqrt{3} \times \sqrt{3}$-*R*30° structure on Pt{1 1 1} [41], with only atop sites occupied.

On Pt{1 1 1} at $\theta > 0.33$, a surface phase transition occurs leading to a $c(4 \times 2)$ structure where half CO molecules are on-top (2094 cm^{-1}) and half bridging (1870 cm^{-1}). Also, on Pt{1 1 0} at higher coverages ($\theta > 0.5$), two bands are observed due to on-top and bridging species (1915 cm^{-1}) [42].

A similar behavior has also been observed for CO adsorbed on Pt{2 1 1} and on Pt{3 3 5} [43], which are constituted by A-steps (or {1 0 0} steps) separating {1 1 1} terraces of different size. Also, in these cases at low coverage, only step on-top adsorbed CO is observed at 2060–2070 cm^{-1}. At higher coverages, terrace on-top CO

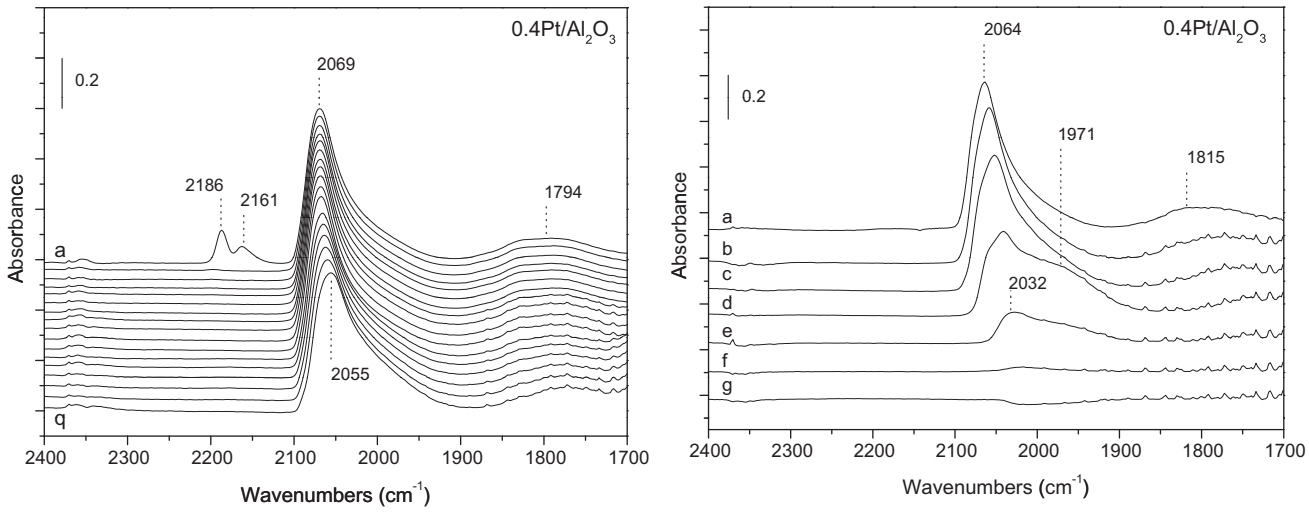

Fig. 3. FTIR spectra of absorbed species arising from CO adsorption over the 0.4Pt/Al_2O_3 catalyst. Left: adsorption at −140 °C; (a) before outgassing, (b–q) outgassing upon warming (−140 °C to 20 °C). Right: adsorption at room temperature; (a) before outgassing, (b) after outgassing, and (c–g) 100–500 °C.

is observed (2085–2100 cm^{-1}) together with bridging species. According to Mukerji et al. [44], a step-bridging species first forms on Pt{2 1 1} (1880–1888 cm^{-1}), followed, at saturation coverage, by a bridging species involving one terrace and one step atom (1918 cm^{-1}). Xu and Yates [37] reported lower frequencies (1845–1855 cm^{-1}) for step-bridging CO on both Pt{2 1 1}and Pt{3 3 5}.

A quite different behavior was observed for CO adsorbed on Pt{1 0 0}. In this case, bridging species appear already at low coverages: IRAS studies on reconstructed Pt{1 0 0}-(1 × 1) show at low coverages bands at 2067 cm^{-1} (atop) and 1870 cm^{-1} (bridging), both shifting to higher frequencies by increasing coverage [45,46].

Baranova et al. [47] investigated by a reflection technique small unsupported Pt particles and observed CO-stretching frequency increasing in the range 2015–2045 cm^{-1} for Pt particle size increasing from 1 to 6 nm. This shows that the CO stretching of adsorbed CO is sensitive to particle size, the smaller the size the lower the stretching frequency.

An absolute prevalence for terminal species with respect to bridging species is also observed in the IR studies of supported Pt catalysts. According to DeMénorval et al. [48], the frequency of terminal CO on Pt–Al_2O_3 catalysts depends on Pt particle size, increasing from 2070 to 2100 cm^{-1} by increasing size from 1 to 10 nm. Raskò [49] concluded that on alumina, monoatomic zerovalent Pt metal may exist, on which CO adsorbs on-top giving rise to νCO at 2117 cm^{-1}. These species can be formed at high CO pressure by reconstruction of Pt particles, when the dominant band due to on-top CO on smooth Pt facets ($d \sim 1$ nm) is observed at 2078 cm^{-1}. At lower CO pressure, bands due to CO adsorbed on edged and kinked Pt atoms of flat Pt particles (2069 and 2041 cm^{-1}) are predominant.

Our data appear to be in substantial agreement with those of both DeMénorval et al. [48] and Raskò [49]. In fact, the positions of terminal carbonyls with respect to the Pt crystal sizes agree with those reported by DeMénorval et al. [48]. We could suppose to have mostly two kinds of particles characterized by a slightly different CO stretching on terminal carbonyls at room temperature, 2075–2032 cm^{-1} and 2064–2032 cm^{-1}. The latter of these two components, indistinguishable upon low-temperature adsorption, disappears by outgassing at 300 °C. It may be assigned to terminal carbonyls on {1 1 1}-like face-exposing particles. The former one, instead, seems to be associated with the band assigned to bridging species, broader, centered near 1940 cm^{-1}. These features behave quite in parallel to outgassing at room or slightly higher temperature. They could be assigned to terminal and bridging carbonyls on Pt{1 0 0}-like face-exposing particles. A restructuring phenomenon upon heating may result in the conversion of Pt{1 1 1}-like face-exposing particles into {1 0 0}-like face-exposing particles at 200–300 °C.

3.5. IR study of CO adsorption over the 4Ni/Al_2O_3 catalyst

The spectra of surface species arising from CO adsorption over the reduced 4Ni/Al_2O_3 catalyst, at low temperature, are presented in Fig. 4, left. In the typical region of carbonyls interacting with metal cations [36], two well-resolved bands were detected at 2184 and 2167 cm^{-1}. These bands appear to be more resistant to outgassing and a little stronger than those observed in the same region on 0.4Pt/Al_2O_3 catalyst. Interestingly, the lower frequency one resists more than the higher frequency one to outgassing, shifting also upwards to 2173 cm^{-1}, which is anomalous for CO interacting with σ-bonds to cationic centers. This suggests that, in the case of the species responsible for the lower frequency band, some additional π-type back-bonding should occur. This allows us to assign with confidence the band at 2184 cm^{-1} to CO adsorbed on Al^{3+} ions (only σ-bonds) and that at 2167–2173 cm^{-1} to CO interacting with Ni^{2+} ions (σ-bonds and π-type back-bonding) like NiO particles or $NiAl_2O_4$ [50,51]. From this observation, it should be pointed out that, even after reduction, some Ni ions resistant to reduction remain over the catalyst surface.

Several quite sharp bands are observed in the lower frequency region, 2150–2000 cm^{-1}, where CO stretchings of terminal carbonyls on reduced metal centers typically occur. The presence of several sharp bands and the almost total absence of bands in the region typical of bridging and triply bridging species (i.e. <2000 cm^{-1}) appear to be more consistent with the formation of polycarbonyl species rather than with CO interacting with metal particles. In fact, CO adsorption on Ni metal particles usually gives rise to low-frequency CO-stretching bands in the region assigned to bridging and triply bridging CO together with and more intense than those due to terminal ones [52]. On Ni{1 1 1} at low coverages, a predominant band is observed shifting from 1830 to 1900 cm^{-1} depending on the coverage, traditionally assigned to bridging CO, and a weaker one at 1796–1825 cm^{-1} usually attributed to hollow adsorbed molecules (triply bridging) together with

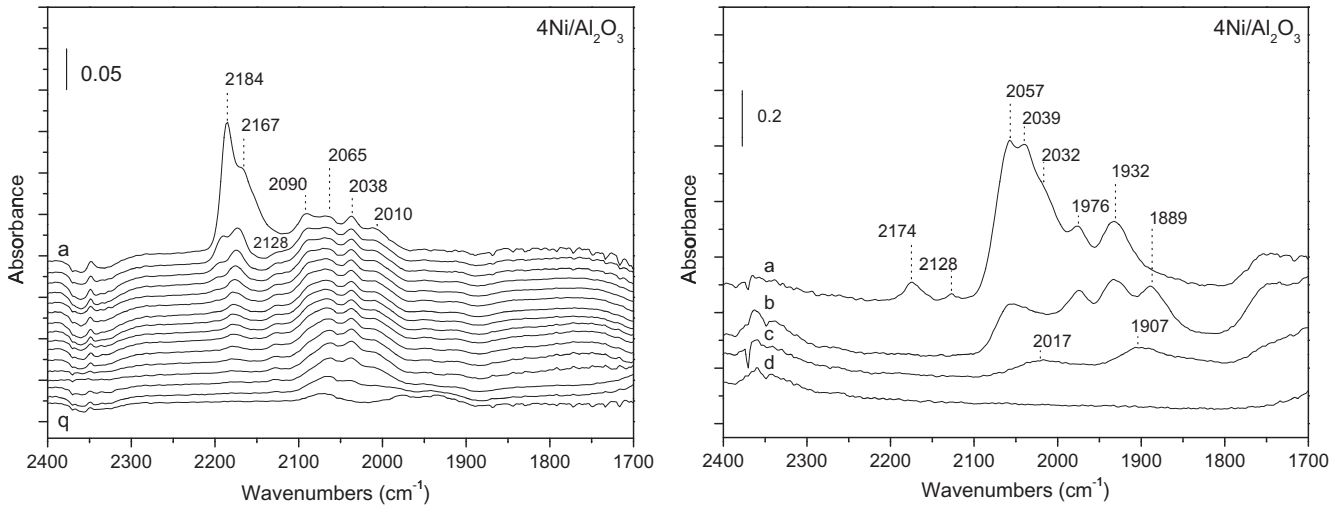

Fig. 4. FTIR spectra of absorbed species arising from CO adsorption over the 4Ni/Al_2O_3 catalyst. Left: adsorption at −140 °C; (a) before outgassing, (b–q) outgassing upon warming (−140 °C to 20 °C). Right: adsorption at room temperature; (a) before outgassing, (b) after outgassing, and (c and d) 100–200 °C.

weak bands due to terminal carbonyls (2030–2060 cm^{-1} depending on the coverage [52]). In fact, more recent structural studies [53,54] show that at increasing coverages, a sequence of different ordered structures, namely p(2 × 2)-(CO), $\sqrt{3} \times \sqrt{3}$-*R*30°-(CO) and c(2 × 4)-(2CO), all implying only triply bridging species (hcp and fcc positions) occurs. A recent DFT study [55] suggested that at half coverage, the two low-frequency bands can be due to in-phase and out-of-phase modes of these structures. Only at higher CO coverage ($\theta > 0.50$), a structure with one on-top and three bridging species forms.

According to Yoshinobu and Kawai [56], on Ni{1 0 0} at 20 K and very low coverage, the bands of terminal and bridging CO are observed at 2019–2029 cm^{-1} and 1863–1875 cm^{-1}, respectively, the latter split at higher coverages. At room temperatures, these features were found at 2016 cm^{-1} and 1935 cm^{-1} [57]. A similar situation was found for CO on Ni{3 1 1} [58].

Also, for high loading and highly reduced alumina-supported Ni catalysts, quite broad bands are usually observed upon CO adsorption at 2080–2020 cm^{-1} and at 1930–1870 cm^{-1} [59–61], typically assigned to terminal and bridging carbonyls on extended Ni metal particles.

Here, several sharp bands detected above 2000 cm^{-1} suggest the formation of Ni polycarbonyl species. The behavior of these bands upon outgassing under warming suggests the existence of a doublet, at 2090 and 2128 cm^{-1}, associated with a more labile species, and a triplet, at 2010, 2038 and 2065 cm^{-1}, assigned to a more resistant species. The doublet at 2090 and 2128 cm^{-1} could be associated with the formation of $Ni^{+}(CO)_2$ complexes, which are typically characterized by adsorption bands at 2145–2130 cm^{-1} and 2100–2081 cm^{-1} [36,62].

The three weak bands at 2010, 2038 and 2065 cm^{-1}, with similar relative intensities, could be due to Ni^0 polycarbonyls, like $Ni(CO)_3$, likely frozen precursors of the formation of $Ni(CO)_4$, which is in fact detected in the gas phase after contact of the catalyst surface with CO at room temperature. This may be an indication of the existence of atomically dispersed zerovalent nickel, as already reported for Ni–YSZ catalysts [63].

Additionally, in the region 1900–2000 cm^{-1}, two really weak shoulders could be distinguished at 1912 and 1947 cm^{-1}, which are associated with the presence of small amounts of bridging species, likely on few sufficiently large Ni^0 particles. After increasing the temperature, these bands increased in intensity and shifted to 1933 and 1973 cm^{-1}, coinciding with the band registered at room temperature.

The spectra of surface species arising from CO adsorption over the reduced $4Ni/Al_2O_3$ catalyst, at room temperature, shown in Fig. 4, right, appear quite different from those observed in the low-temperature adsorption experiment.

In these spectra, in fact, together with several sharp maxima, quite large and strong absorption are observed centered in the regions typical for terminal and bridging carbonyls on extended Ni metal particles [59–61]. After outgassing at 100 °C, i.e. at the lowest coverage, these bands are still evident, although weak, at 2017 and 1907 cm^{-1}, the latter stronger. The overall spectrum is very similar to the one observed for CO adsorbed at r.t. on Ni{1 0 0} [57]. After outgassing at r.t., an additional triplet is observed at 2050, 1976 and 1889 cm^{-1}, which could roughly correspond to the spectrum observed for CO adsorbed on Ni{1 1 1}, assigned to terminal and triply bridging species (antisymmetric and symmetric modes) [52–55]. It seems likely that the formation of extended Ni metal particles in this experiment can be due to a restructuring and agglomeration of Ni species favoured by the intermediate formation of gaseous $Ni(CO)_4$, which is in fact detected by IR (strong band at 2057 cm^{-1}).

Before outgassing, bands associated with CO interacting with both ionic and metallic isolated Ni species can be identified. Ionic species are identified by bands at 2174 cm^{-1}, associated with the presence of Ni^{2+}–CO species, and at 2128 cm^{-1}, which could be due to the higher frequency component of the doublet assigned to $Ni^{+}(CO)_2$ species, ions, where the associated band located around 2090 cm^{-1} could be masked by the stronger absorption at lower frequency. The sharp features at 2057, 2039 and 2032 cm^{-1} could be due to species like physisorbed $Ni(CO)_4$ and $Ni(CO)_3$, as discussed earlier.

The spectroscopic data here discussed, in agreement with literature findings [64] point out the formation of highly isolated and partly ionic Ni centers that tend to aggregate favoured by the evolution of gas-phase $Ni(CO)_4$ already at r.t., producing moderately extended Ni metal particles.

3.6. IR study of CO adsorption over the $0.04Pt4Ni/Al_2O_3$ catalyst

The spectra of surface species arising from CO adsorption over the reduced $0.04Pt4Ni/Al_2O_3$ catalyst, at low temperature, are shown in Fig. 5, left side. In the region of carbonyls interacting with cation centers, 2150–2200 cm^{-1}, two bands at 2156 and 2184 cm^{-1} were registered. After outgassing, two bands are still evident at 2176 cm^{-1} and 2193 cm^{-1}. The lower frequency peak remains in the spectrum even after extensive outgassing of the sample. As discussed earlier, the band shifting from 2184 cm^{-1} toward higher frequencies is confidently assigned to Al^{3+}–CO carbonyls, while that at ca. 2176 cm^{-1} is assigned to Ni^{2+}–CO. The very labile component at ca. 2156 cm^{-1} can be due to CO interacting with surface hydroxyl groups, and/or to Pt^{2+}–CO species. This shows again the presence of unreduced Ni after our reduction treatment.

In the lower frequency region, we can distinguish two bands of species that resist outgassing, although shifted significantly to lower frequencies. The bands at 2089–2060 cm^{-1} and 1938–1925 cm^{-1} seem to resemble more to CO adsorbed on Pt{1 0 0}-like face (as discussed earlier for the $0.4Pt/Al_2O_3$ catalyst spectra), than to CO on Ni metal particles. On the other hand, the three bands at 2067, 2037 and 2012 cm^{-1}, which behave quite in parallel and correspond to a more labile species, are closely similar to those previously assigned to Ni^0 polycarbonyls, like $Ni(CO)_3$.

In Fig. 5, right, the spectra of absorbed species arising from CO adsorption at room temperature over the reduced $0.04Pt4Ni/Al_2O_3$ catalyst are presented. These features are again quite different with respect to those observed in the low-temperature experiment spectra. At high frequency, two weak bands at 2176 and 2127 cm^{-1}, corresponding to very labile species, are assigned again to Ni^{2+}–CO and $Ni^{+}(CO)_2$ species (higher frequency component).

In the lower frequency region, bands typical of terminal and bridging CO over metal crystals, resisting outgassing, can be seen again. This time, however, the maximum of νCO of terminal carbonyls is observed quite split, with one component shifting from ca. 2055 to 2019 cm^{-1}, and another component evident as a shoulder in the 2070–2050 cm^{-1} range. While the former is typical for terminal CO on Ni crystal faces, the latter is more typical of CO on Pt monocrystal faces. This suggests that two kinds of metal particles exist, one of which is Ni rich, the other Pt rich. At lower frequency, a band assigned to bridging species is found also split, with a component near 1930 cm^{-1}, the other near 1889 cm^{-1}, also behaving in a different way. Only at high loadings, a further band at 1977 cm^{-1} can be found. These data suggest that we can find three different kinds of metal surfaces, i.e. a Pt{1 0 0}-like face (2070–2050 cm^{-1} and 1930 cm^{-1}), a Ni{1 0 0}-like face (2019 and ca. 1900 cm^{-1}) and a Ni{1 1 1}-like face (ca. 2050, 1977 and 1889 cm^{-1}). As a comparison, we can cite here that CO adsorption on a $Pt_{25}Ni_{75}$ {1 1 1} monocrystal face has been studied by HREELS [65], showing a main band assigned to terminal surface carbonyls

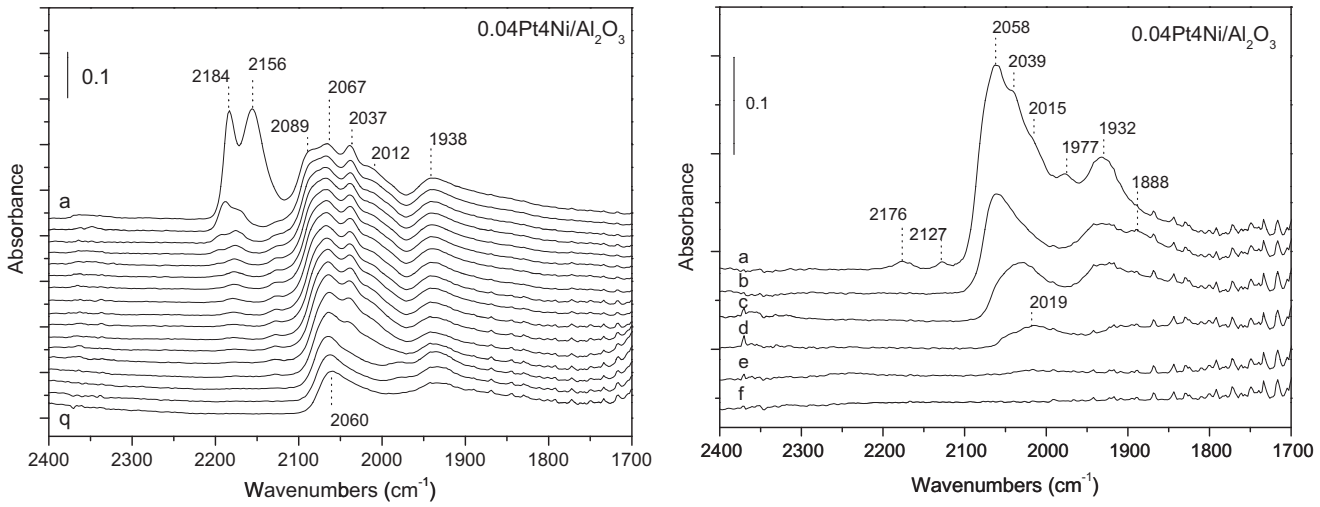

Fig. 5. FTIR spectra of absorbed species arising from CO adsorption over the 0.04Pt4Ni/Al_2O_3 catalyst. Left: adsorption at −140 °C; (a) before outgassing, (b–q) outgassing upon warming (−140 °C to 20 °C). Right: adsorption at room temperature; (a) before outgassing, (b) after outgassing, and (c–f) 100–400 °C.

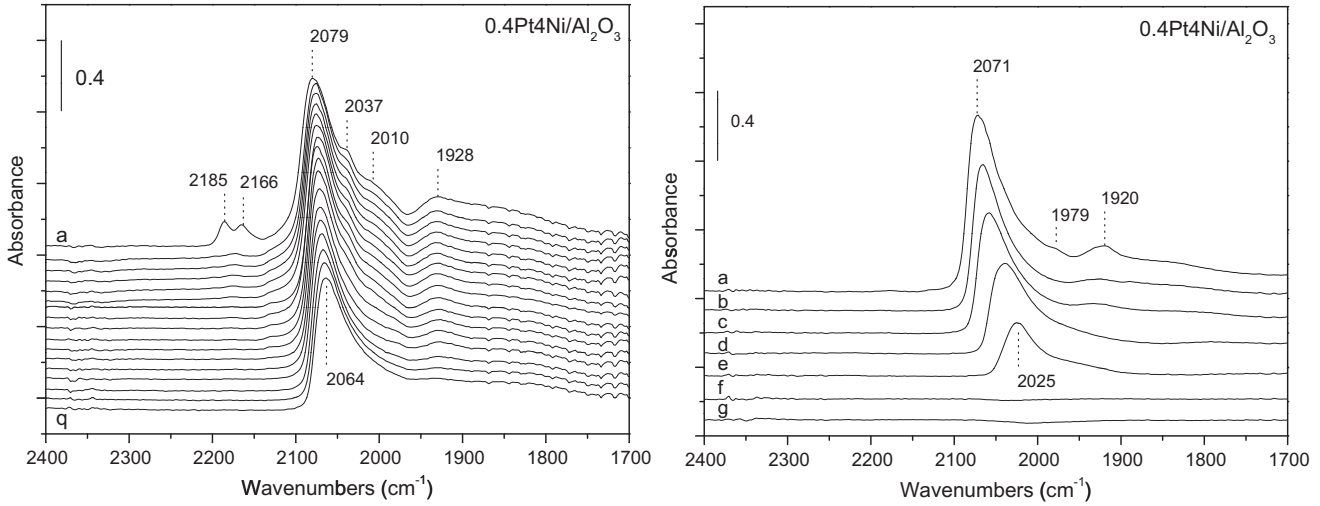

Fig. 6. FTIR spectra of absorbed species arising from CO adsorption over the 0.4Pt4Ni/Al_2O_3 catalyst. Left: adsorption at −140 °C; (a) before outgassing, (b–q) outgassing upon warming (−140 °C to 20 °C). Right: adsorption at room temperature; (a) before outgassing, (b) after outgassing, and (c and g) 100–500 °C.

at 2065 cm^{-1} and, depending on pre-treatment, a weaker band assigned to triply bridging CO on Ni atoms at 1839 cm^{-1}.

The formation of Ni metal particles at room temperature can be again attributed to the role of volatile $Ni(CO)_4$, which allows the agglomeration of Ni atoms.

Also in this experiment, we find at high coverages weak and sharp features at 2058, 2039 and 2015 cm^{-1}, assigned to Ni^0 polycarbonyls, like $Ni(CO)_3$, likely frozen precursors of the formation of $Ni(CO)_4$, which is in fact detected in the gas phase.

3.7. IR study of CO adsorption over the 0.4Pt4Ni/Al_2O_3 catalyst

In Fig. 6, left, the spectra of surface species arising from CO adsorption over the reduced 0.4Pt4Ni/Al_2O_3 catalyst, at low temperature, are presented. The spectra are clearly dominated by a main band shifting from 2079 to 2064 cm^{-1} by increasing temperature upon outgassing, which is definitely similar to that of terminal carbonyls on Pt crystal faces. However, the position of this band is clearly shifted up with respect to that observed on the 0.4Pt/Al_2O_3 catalyst (2069–2054 cm^{-1}). This is certainly an effect of the presence of Ni species. Additionally, a broader band due to a less stable bridging species is found at 1930 cm^{-1}, which can be assigned to bridging CO on Pt{1 0 0}-like particles.

The spectra recorded at room temperature (Fig. 6, right) confirm the existence of terminal carbonyls over a Pt{1 0 0}-like surface, whose νCO is shifting from 2071 down to 2025 cm^{-1}, and weak and labile bridging species whose νCO is centered at 1920 cm^{-1}.

At low temperature (Fig. 6, left) besides these species, other more labile ones can be found, in particular at 2185, 2166, 2037 and 2010 cm^{-1}. The assignment of the band at 2185 cm^{-1} to Al^{3+}–CO carbonyls, and of the bands at 2037 and 2010 cm^{-1} to Ni^0 polycarbonyls, like $Ni(CO)_3$ species, seems straightforward, in agreement to the earlier discussion. The higher frequency component of the triplet is superimposed to the main band. Based on its frequency, the assignment of the band at 2166 cm^{-1}, to either H-bonded CO species or to Pt^{2+}–CO species is likely.

Interestingly, we do not find here the features associated with carbonyl species on unreduced Ni, like Ni^{2+}–CO and $Ni^{+}(CO)_2$, found in the case of 4Ni/Al_2O_3 and 0.04Pt4Ni/Al_2O_3 catalysts. This suggests that, in this case, due to the relevant amount of Pt present,

nickel is more easily reduced. We can remind that XPS data point out that after reaction conditions all Ni-containing catalysts retain Ni largely oxidized. This may be due to the redox character of the dry-reforming reaction, where CO_2 acts as an oxidant and may participate in keeping high the oxidation state of nickel.

4. Discussion

The catalytic data reported here show that the monometallic $0.4Pt/Al_2O_3$ catalyst is slightly more active than the $4Ni/Al_2O_3$ catalyst in the dry reforming of methane, in spite of the smaller metal content, in agreement with the intrinsically higher activity of platinum with respect to nickel in the reaction. However, an improvement in the catalyst activity can be obtained not only by introducing a small amount of Pt on the Ni/Al_2O_3 catalyst ($0.04Pt4Ni/Al_2O_3$ catalyst) but also adding a significant amount of Ni to the Pt/Al_2O_3 catalyst ($0.4Pt4Ni/Al_2O_3$ catalyst). It is evident that some kind of synergy occurs between Ni and Pt on the alumina carrier, improving DRM activity, in terms of conversion. Thus, these elements have a mutual role of activators for each other. However, the most relevant effect that can also have practical application is that the addition of small amounts of Pt significantly decreases the deactivation rate of the catalyst (as discussed in detail elsewhere [28]) by reducing the formation of carbon nanotubes. Thus, small amounts of Pt can be useful to increase catalyst life, thus acting as stabilizer for Ni/Al_2O_3 catalysts.

The data summarized earlier show that the Ni/Al_2O_3 catalyst is largely oxidized not only after mild reduction treatment in the IR cell but also after dry reforming of methane catalytic runs. XPS data show Ni aluminate, whose formation implies a slow reaction at high temperature with the support, as the predominant Ni species. This is typical for a non-noble metal-like nickel. However, these data, which may confirm previous ones reported for Ni-based ethanol steam-reforming catalysts [16,63], suggest that dry-reforming and steam-reforming processes, where actually redox reactions are performed, may involve redox cycles of catalysts, thus involving not only Ni metal but also oxidized Ni centers. In practice, it seems clear that the oxidation state of nickel is flexible in reforming conditions and that nickel may be oxidized at the surface by water and by CO_2, also with the help of the dispersing ability for Ni ions of ionic supports like alumina. As discussed previously [61], this point of view partly contradicts all-metal catalysis, mostly supposed to occur for both reforming and methanation on Ni catalysts, although it is not excluded that two mechanisms can act simultaneously (all metallic and redox).

The difference between room-temperature and low-temperature CO adsorption experiments provide evidence of the formation at r.t. of $Ni(CO)_4$ and of a likely role of this volatile compound of allowing restructuring and coalescence of Ni metal particles at room temperature. This is a case where the use of CO as a probe must be taken with care, because it may have a role in surface modification. The formation of gas-phase $Ni(CO)_4$ has been put in relation to the formation of a sharp and weak triplet during CO adsorption, at ca. 2065, 2038 and 2010 cm^{-1}, with similar relative intensities, assigned to Ni^0 polycarbonyls, like $Ni(CO)_3$, likely frozen precursors of the formation of $Ni(CO)_4$.

As expected, our Pt/Al_2O_3 catalyst appears to be fully reduced both after reaction and after hydrogen treatment in the cell, producing small but well-characterized nanocrystals whose surface appears to be formed by both Pt{1 0 0}-like and Pt{1 1 1}-like faces. A restructuring phenomenon upon heating may result in the conversion of Pt{1 1 1}-like face-exposing particles into {1 0 0}-like face-exposing particles at 200–300 °C.

As for the bimetallic catalysts, it is evident that at least for the $0.4Pt4Ni/Al_2O_3$ sample, a fcc solid solution certainly forms, as previously found for silica-supported Pt–Ni catalysts [31–34]. The application of the Vegard's rule to the data arising from XRD for spent catalyst suggest that the real composition of the solid solution (in terms of Ni to Pt ratio) is similar to that of the virtual composition of the catalyst. However, XPS data suggest that only a small part of nickel is reduced after reaction, thus the metallic Ni to metallic Pt ratio is much lower. IR spectra of adsorbed CO confirm that a solid solution occurs, indicating that the surface appears to be dominated by Pt centers whose electron-withdrawing character is increased by nickel. In fact, the CO-stretching frequency on the alloy is 10 cm^{-1} higher than on pure Pt. On the other hand, the data suggest that the alloy is enriched at the surface by Pt but has also a definitely smaller crystal size than the metal particles on pure Pt and Ni catalyst, and this may be the main reason of higher νCO for terminal carbonyls.

Previous studies reported face-dependent surface enrichment on Pt–Ni alloys: according to these studies, {1 1 1} and {1 0 0} surfaces tend to be Pt-enriched, while {1 1 0} tends to be Ni-enriched [65,66]. In agreement with this, our data suggest that on the bimetallic catalyst a Pt{1 0 0}-like surface is mostly exposed.

In agreement with very recent results reported by Mukainakano et al. [67], in spite of the larger concentration on nickel, the surface of bimetallic $Ni–Pt/Al_2O_3$ catalysts seems to be due to Pt-rich metal surfaces together with mostly dispersed and easily oxidized Ni centers. The addition of platinum, however, favors the formation of even smaller metal particles with respect to pure nickel, thus increasing significantly the electron-withdrawing ability of Pt centers.

The presence of such particles modifies the chemical behavior of Ni, increasing its reducibility as shown by XPS data as well as by Temperature-Programmed Reduction results [68]. The surface enrichment by platinum is at the origin of the lower tendency to form carbonaceous materials, with the result of increasing stability of the catalyst [28] and enhancing slightly the catalytic activity of Ni/Al_2O_3.

Acknowledgments

M.G.D. acknowledges the Spanish Minister of Education and Science for a FPI grant and for the financial support to the projects ENE2004-06176 and ENE2007-67926-C02-02/ALT.

References

[1] J.R. Røstrup-Nielsen, J. Sehested, J.K. Norskov, Adv. Catal. 47 (2002) 66.
[2] R.M. Navarro, M.A. Peña, J.L.G. Fierro, Chem. Rev. 107 (2007) 3952.
[3] J.R. Røstrup-Nielsen, in: J.R. Anderson, M. Boudart (Eds.), Catal. Sci. Technol., vol. 5, Springer, Berlin, 1984, p. 1.
[4] D.E. Ridler, M.V. Twigg, in: M.V. Twigg (Ed.), Catalyst Handbook, second ed., Wolfe pub., London, 1989, p. 225.
[5] K. Takehira, J. Nat. Gas Chem. 18 (2009) 237.
[6] P. Ramírez de la Piscina, N. Homs, Chem. Soc. Rev. 37 (2008) 2459.
[7] A. Haryanto, S. Fernando, N. Murali, S. Adhikari, Energy Fuels 19 (2005) 2098.
[8] P.D. Vaidya, A.E. Rodrigues, Chem. Eng. J. 117 (2006) 39.
[9] M. Ni, D.Y.C. Leung, M.K.H. Leung, Int. J. Hydrogen Energy 32 (2007) 3238.
[10] F. Frusteri, S. Freni, J. Power Sour. 173 (2007) 200.
[11] C. Resini, T. Montanari, L. Barattini, G. Ramis, G. Busca, S. Presto, P. Riani, R. Marazza, M. Sisani, F. Marmottini, U. Costantino, Appl. Catal. A: Gen. 355 (2009) 83.
[12] A.C. Basagiannis, X.E. Verykios, Appl. Catal. A: Gen. 308 (2006) 182.
[13] J.A. Medrano, M. Oliva, J. Ruiz, L. Garcia, J. Arauzo, Int. J. Hydrogen Energy 33 (2008) 4387.
[14] L. Barattini, G. Ramis, C. Resini, G. Busca, M. Sisani, U. Costantino, Chem. Eng. J. 153 (2009) 43.
[15] S. Adhikari, S.D. Fernando, A. Haryanto, Energy Convers. Manage. 50 (2009) 2600.
[16] C. Resini, M.C. Herrera Delgado, S. Presto, L.J. Alemany, P. Riani, R. Marazza, G. Ramis, G. Busca, Int. J. Hydrogen Energy 33 (2008) 3728.
[17] N. Homs, J. Llorca, P. Ramírez de la Piscina, Catal. Today 116 (2006) 361.
[18] C.J. Michael, M. Bradford, A. Vannice, J. Catal. 173 (1998) 157.
[19] J. Wei, E. Iglesia, J. Catal. 224 (2004) 370.

[20] M. Garcia-Diéguez, I.S. Pieta, M.C. Herrera, M.A. Larrubia, I. Malpartida, L.J. Alemany, Catal. Today 149 (2010) 380.
[21] B. Pawelec, S. Demyaniova, K. Arishtirova, J.L.G. Fierro, L. Petrov, Appl. Catal. A: Gen. 323 (2007) 188.
[22] M.M. Bhasin, J.H. McCain, B.V. Vora, T. Imai, P.R. Pujadó, Appl. Catal. A: Gen. 221 (2001) 397.
[23] Süd Chemie, General Catalyst Catalogue, available on the web, www.sud-chemie.com.
[24] B.J. Schiavone, NIPRA 2007 O&A and Technology Forum, 2007.
[25] I. Wender, Fuel Proc. Technol. 48 (1996) 189.
[26] B.B. Pearce, M.V. Twigg, C. Woodward, in: M.V. Twigg (Ed.), Catalyst Handbook, second ed., Wolfe pub., London, 1989, p. 340.
[27] C.D. Wagner, NIST X-ray Photoelectron Spectroscopy Database, Gathersburg, 1989; C.D. Wagner, A.V. Naumkin, A. Kraut-Vass, J.W. Allison, C.J. Powell, J.R. Rumble Jr., NIST Standard Reference Database 20, Version 3.4 <http://srdata.nist.gov/xps/>.
[28] M. García-Diéguez, I.S. Pieta, M.C. Herrera, M.A. Larrubia, L.J. Aleman, J. Catal. 270 (2010) 136.
[29] K. Nagaoka, K. Seshan, K. Aika, J.A. Lercher, J. Catal. 197 (2001) 34.
[30] X.G. Lu, Bo. Sundman, J. Agren, CALPHAD 33 (2009) 450.
[31] J. Arenas-Alatorre, M. Avalos-Borja, G. Diaz, Appl. Surf. Sci. 189 (2002) 7.
[32] C. Raab, J.A. Lercher, J.G. Goodwin Jr., J.Z. Shyu, J. Catal. 122 (1990) 406.
[33] A. Jentys, B. McHugh, G. Haller, J.A. Lercher, J. Phys. Chem. 96 (1992) 1324.
[34] A. Jentys, G.L. Haller, J.A. Lercher, J. Phys. Chem. 97 (1993) 484.
[35] D. Curulla, A. Clotet, J.M. Ricart, F. Illas, J. Phys. Chem. 103 (1999) 5246.
[36] K.I. Hadjivanov, G.N. Vayssilov, Adv. Catal. 47 (2002) 307.
[37] J. Xu, J.T. Yates, Surf. Sci. 327 (1995) 193.
[38] A. Crossley, D.A. King, Surf. Sci. 95 (1980) 131.
[39] G. Rupprechter, H. Unterhalt, M. Morkel, P. Galletto, T. Dellwig, H.-J. Freund, Vacuum 71 (2003) 83.
[40] C. Klünker, M. Balder, S. Lehwald, W. Daum, Surf. Sci. 360 (1996) 104.
[41] P.J. Feibelman, B. Hammer, J.K. Nørskov, F. Wagner, M. Scheffler, R. Stumpf, R. Watwe, J. Dumesic, J. Phys. Chem. B 105 (2001) 4018.
[42] S.R. Bare, P. Hofmann, D.A. King, Surf. Sci. 144 (1984) 347.
[43] J. Xu, J.T. Yates, Surf. Sci. 327 (1995) 193.
[44] R.J. Mukerji, A.S. Bolina, W.A. Brown, Surf. Sci. 527 (2003) 198.
[45] R. Martin, R. Gardner, A.R. Bradshaw, Surf. Sci. 342 (1995) 69.
[46] D. Curulla, A. Clotet, J.M. Ricart, Surf. Sci. 460 (2000) 101.
[47] E.A. Baranova, C. Bock, D. Ilin, D. Wang, B. MacDougall, Surf. Sci. 600 (2006) 3502.
[48] L.C. deMénorval, A. Chaqroune, B. Coq, B. Figueras, J. Chem. Soc. Faraday Trans. 1 (93) (1997) 3715.
[49] J. Raskò, J. Catal. 217 (2003) 478.
[50] G. Busca, V. Lorenzelli, V. Sanchez Escribano, R. Guidetti, J. Catal. 131 (1991) 167.
[51] G. Busca, V. Lorenzelli, V. Sanchez Escribano, Chem. Mater. 4 (1992) 595.
[52] M.A. Vannice, in: J.R. Andeson, M. Boudart (Eds.), Catal. Sci. Technol., vol. 3, Springer Verlag, 1982, p. 139.
[53] G. Held, J. Schuler, W. Sklarek, H.-P. Steinrück, Surf. Sci. 398 (1998) 154.
[54] W. Braun, H.-P. Steinrück, G. Held, Surf. Sci. 575 (2005) 343.
[55] A. Eichler, Surf. Sci. 526 (2003) 332.
[56] J. Yoshinobu, M. Kawai, Surf. Sci. 363 (1996) 105.
[57] V. Formoso, A. Marino, G. Chiarello, R.G. Agostino, T. Caruso, E. Colavita, Surf. Sci. 600 (2006) 1456.
[58] P. Schilbe, S. Siebentritt, K.-H. Rieder, Chem. Phys. Lett. 233 (1995) 569.
[59] L. Kubelková, J. Nováková, N.I. Jaeger, G. Schulz-Ekloff, Appl. Catal. A: Gen. 95 (1993) 87.
[60] S. Derrouiche, D. Bianchi, Appl. Catal. A: Gen. 313 (2006) 208.
[61] V. Sanchez Escribano, M.A. Larrubia Vargas, E. Finocchio, G. Busca, Appl. Catal. A: Gen. 316 (2007) 68–74.
[62] K. Hadjiivanonv, H. Knözinger, M. Mihaylov, J. Phys. Chem. B 106 (2002) 2618.
[63] C. Resini, T. Venkov, K. Hadjiivanov, S. Presto, P. Riani, R. Marazza, G. Ramis, G. Busca, Appl. Catal. A: Gen. 353 (2009) 137.
[64] G. Poncelet, M.A. Centeno, R. Molina, Appl. Catal. A: Gen. 288 (2005) 232.
[65] A. Pandförder, J. Skonieczny, E. Janssen, G. Meister, A. Goldmann, P. Varga, Surf. Sci. 331-333 (1995) 824.
[66] P. Weigand, B. Jelinek, W. Hofer, P. Varga, Surf. Sci. 307-309 (1994) 416.
[67] Y. Mukainakano, K. Yoshida, S. Kado, K. Okumura, K. Kunimori, K. Tomishige, Chem. Eng. Sci. 63 (2008) 4891.
[68] M. Garcia-Diéguez, I.S. Pieta, M.C. Herrera, M.A. Larrubia, L.J. Alemany, Appl. Catal. A: Gen. 377 (2010) 191.